Maternal–Fetal In Vivo Imaging: A Combined PET and MRI Study

Helene Benveniste, MD, PhD[1,2]; Joanna S. Fowler, PhD[3]; William D. Rooney, PhD[3]; Daryn H. Moller, MD[2]; W. Walter Backus, MD[2]; Donald A. Warner[3]; Pauline Carter, RN[1]; Payton King[1]; Bruce Scharf, DMV[1,4]; David A. Alexoff, BSE[3]; Yeming Ma, PhD[1]; Paul Vaska, PhD[3]; David Schlyer, PhD[3]; and Nora D. Volkow, MD[1]

[1]Medical Department, Brookhaven National Laboratory, Upton, New York; [2]Department of Anesthesiology, State University of New York Stony Brook, Stony Brook, New York; [3]Chemistry Department, Brookhaven National Laboratory, Upton, New York; and [4]Division of Laboratory Animal Resources, State University of New York Brooklyn, Brooklyn, New York

An understanding of how drugs are transferred between mother and fetus during the gestational period is an important medical issue of relevance to both therapeutic drugs and drugs of abuse. Though there are several in vitro and in vivo methods to examine this issue, all have limitations. Furthermore, ethical and safety considerations generally preclude such studies in pregnant humans. PET and appropriately labeled compounds have the ability to provide information on both maternal–fetal drug pharmacokinetics and pharmacodynamics. We present here a nonhuman primate animal model and the methodology for combining PET and MRI to identify fetal organs and to measure maternal and fetal isotope distribution using ^{18}F-FDG and a whole-body imaging protocol to demonstrate proof-of-principle. **Methods:** One nonpregnant nonhuman primate was used for determination of the anesthesia protocol and MRI methods and 3 pregnant nonhuman primates (*Macaques radiata*) weighing 4.5–7 kg were used for the imaging study and anesthetized with propofol (160–300 μg/kg/min). Anatomic T2-weighted MR images were acquired on a 4-T MR instrument. Subsequently, whole-body PET images were acquired 35 min after injection of ^{18}F-FDG, and standardized uptake values (SUVs) were calculated. Image processing and coregistration were performed using commercial software. **Results:** All animals underwent uneventful general anesthesia for a period of up to 7 h. Coregistration of PET and MR images allowed identification of fetal organs and demonstrated that ^{18}F-FDG readily crosses the placenta and that ^{18}F accumulates in both maternal and fetal brain, heart, and bladder. Brain SUVs averaged 1.95 ± 0.08 (mean ± SD) and 1.58 ± 0.11 for mothers and fetuses, respectively. Monkeys delivered healthy babies after a normal gestational term of 170 d following the PET/MRI study. **Conclusion:** The pregnant macaque in combination with PET and MRI technology allows the measurement of radioisotope distribution in maternal and fetal organs. This demonstrates the potential for noninvasively measuring the transfer of drugs across the placenta and for measuring the fetal drug distribution. It also opens up the possibility for studying binding and elimination as well as the effects of a drug on specific cellular elements and physiologic processes during the gestational period in a primate model.

Key Words: maternal–fetal exchange; imaging; in vivo; primate

J Nucl Med 2003; 44:1522–1530

Research in the area of maternal–fetal exchange has been the focus of investigators for several decades (*1–7*). The need to understand and characterize how nutrients, metabolites, pharmaceuticals, and (potential) toxins are exchanged between mother and fetus during the gestational period is essential for several reasons. First, knowledge of the bidirectional maternal–fetal exchange of nutrients and metabolites is critical to understand fetal physiology, metabolism, normal fetal growth patterns, and overall fetal maturation. Second, if medical treatment is warranted during pregnancy, it is paramount to know if and how drugs are transferred from mother to fetus; how the drugs are distributed, metabolized, and eliminated by the fetus; and how drugs affect the fetus. For example, if the mother is the patient, maternal transfer of drugs to the fetus may be hazardous. On the other hand, if the fetus is the patient, sufficient transplacental transfer of drugs from the mother to the fetus becomes crucial in regard to therapeutic efficacy. Third, maternal transfer of substances of abuse such as nicotine, alcohol, cocaine, heroin, and methamphetamine is another area of escalating importance (*8–11*). Thus, several drugs of abuse gain access into the maternal circulation during pregnancy through either involuntary or voluntary exposure. The potential transfer of these compounds into the placenta and the fetus is a serious health concern.

The exchange of compounds across the placenta occurs by concentration gradient–dependent diffusion as well as by active transport by specific transporters that are expressed in the maternal-facing border of the placenta and the fetal-facing basal membrane of the syncytiotrophoblast (*12*). These transporters can carry across physiologic, endogenous substrates as well as nonphysiologic exogenous compounds (e.g., pharmaceuticals, toxins, drugs of abuse, or

Received Jan. 21, 2003; revision accepted May 1, 2003.

For correspondence or reprints contact: Helene Benveniste, MD, PhD, Medical Department, Bldg. 490, Brookhaven National Laboratory, 30 Bell Ave., Upton, NY 11793.

E-mail: benveniste@bnl.gov

environmental pollutants) (*12*). Placental exchange of substances can also occur by bulk flow (hydrostatic gradient) or by pinocytosis.

Because of ethical and safety issues, the study of maternal–fetal transfer in humans is limited to several in vitro and in vivo techniques. In vitro techniques include the dually perfused human placental cotyledon, placental tissue slices, syncytiotrophoblast tissue preparations, and cultured human placental villus tissues and cells (*6*). Determination of placental exchange of drugs can also be assessed in vivo by calculating the ratio of fetal-to-maternal blood drug concentration. Further, by also measuring the concentration of the compound in the umbilical artery (at the time of delivery), information in regard to fetal drug metabolism and elimination can be obtained. For example, in a recent study, the placental transfer of remifentanil (a drug with μ-specific opioid activity) and its metabolite was determined after a continuous intravenous infusion to the mother (steady state) (*13*). Maternal arterial (MA), umbilical arterial (UA), and umbilical venous (UV) blood samples were obtained at delivery (*13*). The mean remifentanil UV:MA ratio of 0.88 suggested significant placental transfer, and the remifentanil UA:UV ratio of 0.29 suggested either rapid metabolism or rapid redistribution of the drug in the fetus (*13*). Another in vivo approach is to also measure the concentration of drug in the amniotic fluid (*14*). Amniotic fluid is produced by the fetus (urine production, lung secretions, and oral–nasal secretions) as well as by the placenta (amniotic fluid exchanges with the vasculature of the amniochorion) (*15*). Thus, the presence of a given drug of interest in the amniotic fluid indicates transfer of the drug across the placenta and fetal exposure (*15*). Alternatively, in animal models, maternal–fetal drug transfer can be studied by administering the drug to the mother and subsequently measuring the drug concentration directly in the fetal organs after sacrifice (*16*).

All of the in vitro techniques described above allow examination of transfer of substances across the placenta but do not yield information in regard to (a) how the drugs are metabolized, distributed, and eliminated by the fetus or (b) how the drugs affect the fetus physiologically. On the other hand, the in vivo techniques provide information in regard to transplacental transfer, fetal drug metabolism, and clearance (to a limited extent) but only allow assessments to be made at the time of delivery or termination of pregnancy. Further, none of the techniques address other pharmacokinetic (the study of the time course of drug and metabolite levels in different fluids, tissues, and excreta of the body and of the mathematic relationships required to develop models to interpret such data) and pharmacodynamic (the study of the biochemical and physiologic effects of drugs and their mechanisms of action) parameters such as the time course of drug and metabolite levels in different fetal fluids, tissues, and excreta or the action of a drug in the fetus over a period of time.

The combination of imaging technologies such as PET and MRI would allow noninvasive detection of maternal–fetal transfer of drugs and fetal drug distribution and elimination as well as the identification of fetal organs. For example, with a radiolabeled drug of interest, maternal or fetal drug distribution ratios could be measured regionally, providing that fetal organs could be identified and spatially resolved by the PET scanner. Additionally, for suitable receptor ligands, receptor-binding characteristics could be assessed in fetal brain and other organs.

For safety reasons, radioisotope techniques are precluded in pregnant women with rare exceptions in the pregnant cancer patient (*17*). However, the pregnant nonhuman primate—compared with other animal species such as rodents or sheep—is a potentially more clinically relevant model to use for the assessment of drug pharmacokinetics and pharmacodynamics in the living mother and fetus. In fact, there is precedent for using PET in pregnant monkeys to visualize placental transfer of nutrients (^{11}C-methionine) (*18*) and drugs (^{11}C-morphine metabolites and ^{11}C-heroin) in pregnant rhesus monkeys (*19*). For example, Hartvig et al. sampled maternal blood, urine, amniotic fluid, and umbilical vein blood from the fetus and measured ^{11}C activity while imaging the monkey's uterus (*19*). Although some interpretation of pharmacokinetics could be made for ^{11}C-heroin and other compounds with regard to the placenta, it was difficult to identify fetal organs in this study because of the lack of spatial resolution in the PET images and, thus, limited fetal anatomic information. To our knowledge, the concept of using PET imaging technologies to study maternal–fetal exchange and fetal pharmacokinetics by Hartvig et al. in 1989 has not been pursued by other investigators. This is surprising as this approach represents a powerful tool for investigation of maternal–fetal exchange and fetal drug metabolism and because this is an important medical issue. We, therefore, designed a series of experiments in pregnant nonhuman primates (*Macaques radiata*) to revive and improve the previous study design. Through a combined approach of novel anesthesia and physiologic monitoring technologies, MRI, and a higher resolution whole-body PET scanner, we investigated placental transfer and maternal and fetal anatomic distribution of ^{18}F-FDG. ^{18}F-FDG was chosen for these exploratory studies because of its relative stability in brain and heart after an initial uptake period and our prediction that there would be sufficient ^{18}F accumulation in fetal brain and other organs such as heart and bladder to demonstrate proof-of-principle.

MATERIALS AND METHODS

The experimental protocol was approved by the Brookhaven National Laboratory (BNL) and State University of New York (SUNY) Downstate Institutional Animal Care and Use Committees, both accredited by the American Association for Accreditation of Laboratory Animal Care. Four female Bonnet macaques (*M. radiata*), who were group-housed (obtained from the Primate Laboratory, Department of Psychiatry of SUNY Downstate), were used in this study. Two of the 4 monkeys were judged to be in third-trimester gestational stage and 1 was judged to be in early

second-trimester gestational stage by the veterinarian after a brief physical examination, which was performed at the Primate Laboratory under ketamine anesthesia (8 mg/kg intramuscular injection) (Table 1). One nonpregnant monkey was used only to predetermine the anesthesia protocol and MRI parameters and was not exposed to PET imaging (Table 1). The monkeys were transported to BNL 3 wk before the study and were housed in stainless steel cages in air-conditioned, temperature- and light-cycle–controlled rooms according to National Institutes of Health guidelines at the BNL vivarium.

Anesthesia and Physiologic Monitoring for Imaging

In preparation for imaging, the animals were initially anesthetized with an intramuscular injection of ketamine (10 mg/kg) and glycopyrrolate (0.02 mg/kg) using a squeeze cage. The vocal cords were sprayed with cetacaine spray to prevent laryngospasm before intubation with a 2.5–3.0 endotracheal tube (the 3.5 endotracheal tubes were cuffed and the cuff was inflated with air when positioned endotracheally). The endotracheal tube was secured, and correct tube placement was confirmed by auscultation and the presence of end tidal CO_2 ($ETCO_2$). An intravenous line was established in an upper extremity or saphenous vein using a 22-gauge intravenous catheter. Intravenous hydration was provided using Hextend (high-molecular-weight hydroxyethyl starch 6% [Hetastarch; BioTime, Inc.] in buffered electrolyte dextrose solution, 5–10 mL/kg) administered in 10-mL boluses over the 6-h time course. Routine monitors (noninvasive blood pressure, electrocardiography, O_2 saturation probe, and rectal thermometer) were placed. Mechanical ventilation was initiated using a Harvard ventilator (Inspira, Advanced Safety Ventilator; volume controlled) at a fraction of inspired oxygen of 60%–70%. The minute ventilation was adjusted to achieve $ETCO_2$ values of approximately 30 mm Hg. With careful attention to physiologic parameters, a continuous infusion of propofol (Diprivan; AstraZeneca) was started using a microinfusion pump (Baxter, model AS50) at a beginning dose of 120 μg/kg/min. The propofol infusion was adjusted (120–300 μg/kg/min) to maintain the animal at an adequate anesthetic depth (unresponsive to the presence of the endotracheal tube and mechanical ventilation as well as physiologically stable). No muscle relaxation was used.

Transport

The PET and MRI facilities at BNL are located in separate buildings; therefore, transport of the anesthetized macaques was required. For transport, a nonrebreathing circuit with a manual ventilation assistance device (self-inflating bag) and O_2 flowing at 7 L/min was attached to the end of the endotracheal tube and manual ventilation was initiated. The animal was wrapped in warm blankets and positioned in left lateral decubitus (to avoid hypotension) within a specially designed open transport cage. The anesthesiologist monitored the heart rate and respiratory rate continuously during transport. Preparation and transport between the facilities each required approximately 10–15 min.

MRI

All MR images were obtained on a 4.0-T MR instrument (Varian). The animal was positioned in lateral decubitus and routine MRI-compatible monitors were reattached. Mechanical ventilation was continued using the Harvard ventilator (Inspira, Advanced Safety Ventilator; volume controlled) positioned at an appropriate distance from the magnet (6.71-m inspiratory and expiratory tubing were designed for this purpose). Minute ventilation was adjusted to ensure normal oxygenation and ventilation. Vitamin E capsules that were to serve as external fiducial markers on the MR images were positioned directly on the skin using topical skin adhesive (DERMABOND; Closure Medical) in the areas of the abdomen and pelvis. The animal was wrapped in warm blankets and positioned within a quadrature 25-cm coil for radiofrequency transmit and receive so that the lower abdominal and pelvic regions were centered within the coil. Several MR parameters (MR contrast, spatial resolution, imaging plane, total scan time, and breathing motion correction) were applied to define optimal MR scan parameters (Table 2). Scan-synchronous ventilation was implemented during imaging of monkey B57 (Table 2) to evaluate the overall effect of motion control when imaging the anesthetized animals. The raw data were reconstructed by Fourier transform and displayed as magnitude images.

PET Imaging

PET scanning was performed on an ECAT EXACT HR+ scanner (CTI, Inc.), which has a National Electrical Manufacturers Association resolution of 4.6-mm full width at half maximum (FWHM) transaxially and 4.2 mm axially at the center of the field of view. A standard clinical whole-body protocol provided by the PET camera manufacturer was used in the following manner. The pregnant bonnet macaque was positioned in lateral decubitus. Fiducial markers for PET consisting of 74–148 kBq (2–4 μCi) each of ^{18}F in 10 μL applied to Band-Aids (Johnson & Johnson) were taped onto the vitamin E capsules fastened on the monkey's body to facilitate coregistration of the MR and PET images. Scanning was started 35 min after injection of 54.76–91.02 MBq (1.48–2.46 mCi) ^{18}F-FDG prepared according to the method of Hammacher et al. (*20*). Imaging was initiated at the lower section of the mother's pelvis and progressed cephaladly. Data were

TABLE 1
Experimental Subjects

Animal	Body weight (kg)	Age (y)	Pregnant	Gestational stage*	MRI	^{18}F-FDG PET	Injected dose	
							MBq	mCi
BH3	7.0	23	No	—	Yes	No	—	—
Y40	7.0	5	Yes	89/170	Yes	Yes	91.02	2.46
BY38	5.0	2	Yes	147/170	Yes	Yes	54.76	1.48
B57	4.5	2	Yes	145/170	Yes	Yes	56.24	1.52

*Gestational period of *M. radiata* is known to be 170 d. We estimated gestational stage at time of experiment by calculating number of days from day of imaging to delivery of baby.

TABLE 2
MR Parameters

Animal	MR contrast	Sequence	TE/TR	Spatial resolution (mm^3)	Imaging plane	Gating
BH3	Proton density	Spin echo, multislice	20/5,000	0.859 × 0.859 × 4.0	Axial	No
	T2	Spin echo, multislice	50/5,000	1.0 × 0.75 × 4.0	Axial	No
	T2	Fast spin echo	50/8,000	0.859 × 0.859 × 4.0	Axial	No
Y40	Proton density	Spin echo, multislice	20/5,000	0.859 × 0.859 × 3.0	Axial	No
BY38	Proton density	Spin echo, multislice	20/5,000	0.859 × 0.859 × 4.0	Axial	No
	T2	Spin echo, multislice	20/5,000	0.859 × 0.859 × 3.0	Axial	No
B57	T2	Spin echo	50/2,400	1.25 × 1.25 × 2	Coronal	Yes
		Multislice	50/6,000	0.859 × 0.859 × 2	Axial	No
			50/5,000	1.25 × 1.25 × 2	Coronal	Yes
	T2*	Gradient echo, multislice	6.5/100	1.04 × 1.56 × 5	Coronal	No

TE = echo time; TR = repetition time.

acquired using 5 bed positions. For each bed position, transmission data was acquired for 4 min followed by 8 min of emission data. The transmission data were collected with septa extended (2 dimensions) and then segmented to reduce statistical noise as well as bias from emission contamination. Emission data were also collected in 2 dimensions to minimize acceptance of scattered events, axial sensitivity variations, and the overhead time from septa movement between emission and transmission scans (therefore reducing anesthesia exposure to the mother and fetus). Emission data were reconstructed using the vendor-supplied iterative algorithm (attenuation-weighted ordered-subsets expectation maximization with 2 iterations and 8 subsets) and postfiltered with an 8-mm FWHM gaussian kernel. ^{18}F concentration (Bq/mL [nCi/mL[) was obtained by summing the planes in groups of 2 and selecting regions on 2–5 planes and averaging the values in the planes. ^{18}F accumulation in organs (Bq/mL [nCi/mL]) was normalized to the decay-corrected injected activity (MBq [mCi])/maternal body weight (grams) to provide standardized uptake values (SUVs) calculated as ([activity in tissue in Bq/mL (nCi/mL)]/[injected dose in Bq (nCi)]/[body weight (g)]) for the mother and the fetus. These were compared assuming that the ^{18}F label is intracellularly trapped during the initial 35-min uptake period before scanning and remains constant during the whole-body scanning. Ideally, fetal SUVs would be calculated by normalizing fetal organ PET measurements to decay-corrected ^{18}F activity delivered across the placenta to the fetus/fetal body weight. Because accurate determinations of fetal body weight and ^{18}F fetal dose were not practical, fetal SUVs were calculated using maternal dose and body weight. We realize that this is not a typical approach and that, using this approach, we are treating the fetus as a maternal body organ. All values are decay corrected back to time of injection. All 3-dimensional (3D) PET images were displayed using a combination of ECAT 7.2 (CTI, Inc.) and Amira 2.3 (TGS) software.

Image Analysis

The multislice MR datasets were displayed as isotropic 3D volumes using interpolation software (Amira 2.3). Anatomic regions of interest were manually outlined using the Amira image segmentation editor, which allowed for interactive segmentation of the 3D data and quantitative analysis. Fetal interorgan distances (from the center of the 3D reconstructed body organs) were also measured.

PET 3D datasets were displayed as isotropic, color-coded volumes. In the 3 pregnant macaques, the maternal brain, heart, spinal column, and bladder were easily identified on the whole-body PET images. The gravid uterine cavity was clearly visible in the 2 third-trimester macaques. However, fetal structures within it were not clearly decipherable on the PET images, and it was therefore necessary to coregister the PET data with the corresponding MR images to anatomically identify fetal structures with high ^{18}F uptake concentration. The coregistration process included several computational steps (Fig. 1). First, corresponding PET and MRI 3D datasets were displayed side by side. Corresponding external fiducial markers (3 sets of vitamin E capsules on MR images and corresponding ^{18}F markers on PET images) were identified and marked on both datasets using the Landmarkset module (TGS, Inc.; www.TGS.com); internal landmarks (15 internal landmarks) such as maternal kidneys, different areas of the maternal spine, and several points in the outline of the uterine cavity were also used as landmarks (Fig. 1). The marked MRI dataset was subsequently "warped" to the corresponding marked PET dataset that served as the master template. The warped MRI 3D data were displayed in an overlaid fashion with the corresponding master PET 3D dataset to assess the localization of the ^{18}F hot spots within the uterine cavity. Using the coregistered images as references, the ^{18}F concentration was subsequently measured (Bq/mL [nCi/mL]) using CTI software in maternal and fetal body organs in the macaques. Additionally, fetal interorgan distances were measured on the PET images.

RESULTS

The mean arterial blood pressure (MABP) and heart rate (HR) did not change significantly during the 6- to 7-h course of the study (MABP ≈ 60–70 mm Hg; HR ≈ 120–140 beats/min). In the MR scanner the body temperature of all of the macaques decreased 1.0°C–1.5°C, but it was rapidly normalized (36°C–37°C) in the PET scanner before injection of the radiotracer. In 1 animal, the propofol infusion had to be increased repetitively to maintain adequate anesthesia depth, but the animal remained hemodynamically stable even at propofol infusion rates of 300 μg/kg/min.

All the animals survived the procedures. One pregnant animal had an episode of laryngospasm immediately after extubation but this did not result in adverse clinical outcome. Two of the 3 pregnant monkeys delivered full-term normal babies (as evaluated by the veterinarian) approxi-

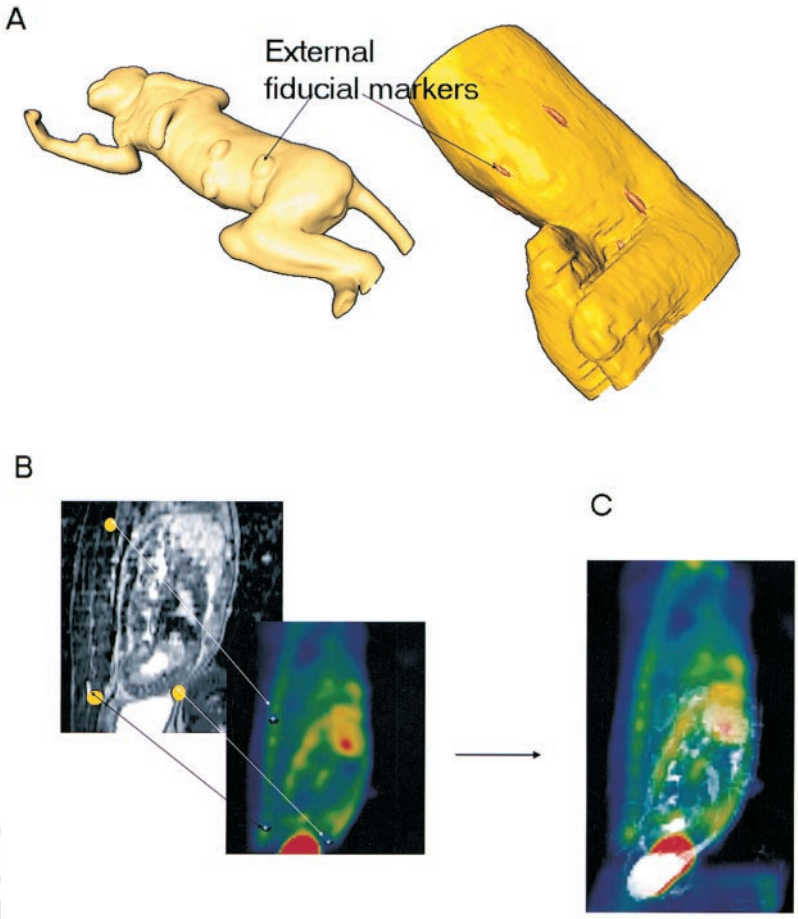

FIGURE 1. PET and MRI coregistration computational process. (A) First step: visualization of external fiducial markers using surface reconstruction algorithm. On left is 3D volume- and surface-rendered display of PET whole-body data; on right are corresponding MRI data. (B) Second step: positioning of corresponding external and internal landmarks on two 3D datasets. (C) Third step: rigid warp and overlay of warped 3D dataset onto PET data. A total of 18 pairs of external and internal landmarks was used to coregister data.

mately 25 d after the imaging experiment. Thus, with a known 170-d gestation period, both of these monkeys were imaged at gestation day 145, signifying third trimester. One monkey, imaged early in pregnancy, delivered a healthy baby on December 28, 2002, indicating early second trimester at the time of imaging (Oct. 1, 2002).

Maternal body organs and the externally positioned fiducial markers (vitamin E capsules) were readily identified on proton density and T2-weighted MR images (Figs. 1 and 2). In the 2 third-trimester fetuses, internal organs such as brain, heart, lungs, liver, intestine, and bladder were clearly displayed on the T2-weighted MR images (Fig. 2). One fetus was in breech position (BY38), whereas the other fetus presented in correct vertex position (B57). The placenta appeared as a low-signal-intensity structure; in fetus B57 the placenta was positioned in the upper uterine segment, and in fetus BY38 it was position laterally. The fetal brain emerged as a homogeneous structure with no microanatomic detail on T2-weighted MR images. The posterior lobe and cerebellum could be identified in fetus B57 (Fig. 2). Both maternal and fetal bladders were bright appearing on the T2-weighted images due to the presence of urine. On T2-weighted and proton density MR images, amniotic fluid also appeared as areas of high signal intensity within the uterine cavity. Crown-rump length was measured (midsag-

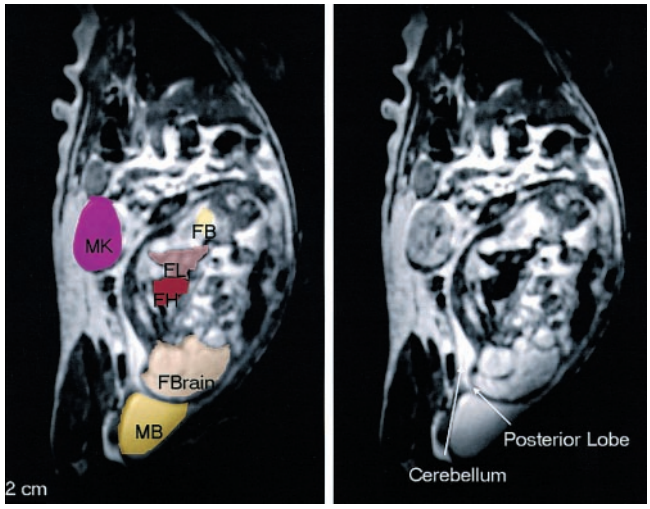

FIGURE 2. T2-weighted MR image of pregnant monkey B57 (third-trimester gestational stage). Maternal and fetal organs are easily recognized. Manual segmentation of organ of interest is displayed: MK = maternal kidney; MB = maternal bladder; FBrain = fetal brain; FH = fetal heart; FL = fetal liver; FB = fetal bladder.

TABLE 3
Measurements of Fetal Organs and Interorgan Distances

Fetus	Crown-rump length (cm)	Brain volume (cm^3)	Heart volume (cm^3)	Liver volume (cm^3)	Brain–bladder distance (mm) MRI/PET
BY38	11.8	36.1	2.9	7.6	97/94
B57	12.7	36.9	3.8	11.3	89/91
Y40	5.0	—	—	—	—

ittally from the 3D dataset) taking the fetal spinal curvature into account. The crown-rump length of BY38 and BY7 fetuses was 11.8 and 12.7 cm, respectively. The fetal crown-rump length of macaque Y40 only measured 5.0 cm, indicative of the early gestational stage. Table 3 presents fetal organ volumes and interorgan distances in the 2 third-trimester fetuses.

As can be seen from Table 4, SUVs for maternal brain (forebrain and cerebellum) and myocardium were within similar ranges for the 3 pregnant macaques, whereas SUVs for maternal kidneys and intestine were variable. The coregistered PET and MRI images of the 2 third-trimester macaques demonstrated that structures of high ^{18}F accumulation within the uterine cavity were localized to fetal brain, heart, and bladder (Fig. 3). The SUVs in the fetal brains were within the same range in spite of the fact that 2 were in the third trimester and 1 was in the second trimester. Myocardial SUVs for the 2 third-trimester fetuses were also similar. Figure 3 shows that the ^{18}F uptake in the fetal brain was heterogeneous with the highest activity in the fetal cerebellum and forebrain. Interestingly, the maternal-to-fetal brain ^{18}F activity ratio was nearly identical for the 2 third-trimester fetuses. ^{18}F activity corresponding to amniotic fluid-rich areas was very low (results not shown). Interorgan distances measured in the 2 third-trimester fetuses were identical to those measured on corresponding MR images (Table 3).

TABLE 4
Comparison of ^{18}F Uptake in Maternal and Fetal Organs After Intravenous Injection of ^{18}F-FDG into 3 Pregnant Macaques

Animal	Organ	Mother	Fetus	Mother/fetus ratio
B57 (3rd trimester)	Forebrain	1.98	1.61	1.23
	Cerebellum	2.02	1.36	1.48
	Heart	1.05	1.22	0.86
	Colon	1.66		
	Kidney	1.34		
	Bladder	14.6	1.48	9.86
BY38 (3rd trimester)	Forebrain	2.01	1.46	1.37
	Cerebellum	2.19	1.60	1.36
	Heart	1.25	1.22	1.02
	Colon	2.38		
	Kidney	1.19		
	Bladder	12.62	1.11	11.36
Y40 (2nd trimester)	Forebrain	1.86	1.67	1.11
	Cerebellum	2.12		
	Heart	1.45		
	Colon	5.99		
	Kidney	3.12		
	Bladder	68.29		

Uptakes are expressed as SUV ([Bq/mL (nCi/mL)]/[Bq (nCi)]/[body weight (g)]).

DISCUSSION

We applied ^{18}F-FDG PET and MRI technologies in pregnant nonhuman primates to examine the feasibility of conducting studies in vivo of maternal–fetal placental transfer of radiolabeled compounds, fetal organ distribution of radiolabeled compounds, and anatomic coregistration using MRI. Our study revealed several findings. First, the anesthesia protocol we developed provided a stable physiologic environment and complete functional recovery of mother and fetus (as evidenced by no preterm labor or deliveries)

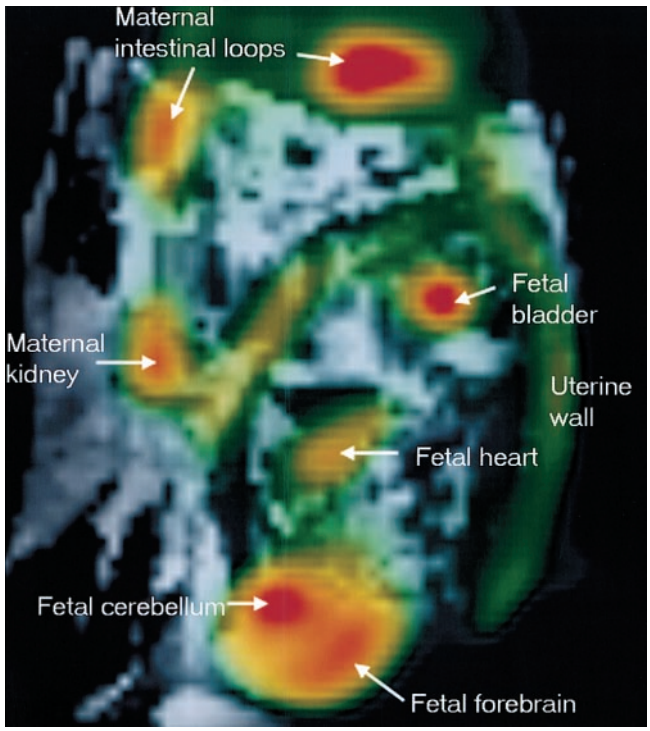

FIGURE 3. Coregistered PET and MRI data of monkey B57. High ^{18}F activity was localized to maternal intestine, maternal kidney, fetal brain, fetal heart, and fetal bladder. Additionally, uterine wall was associated with increased ^{18}F activity.

after >7 h of experimental time, which included multiple transports. Second, T2-weighted MRI with scan-synchronous ventilation provided excellent signal-to-noise ratios (SNRs) and contrast-to-noise ratios with a volume resolution of 2.2–3.1 mm^3. In the third trimester, pregnant nonhuman primates, fetal and surrounding maternal body organ structures were readily identified on T2-weighted MR images. Third, spatial coregistration of PET images with corresponding MR images was enabled with externally positioned fiducial markers and internal maternal structures; MRI/PET coregistered images revealed that ^{18}F activity within the uterine cavity was localized to fetal brain, heart, and bladder. Measurement of ^{18}F activity in maternal and fetal organs revealed similar maternal-to-fetal SUV ratios in the brain of the 2 third-trimester pregnant macaques. Finally, and most importantly, our study provides proof-of-concept that combined PET and MRI can be applied in pregnant nonhuman primates to identify fetal brain and other organs and to study the transfer and distribution of radiolabeled compounds.

PET was first introduced as an imaging tool to study maternal–fetal nutritional exchange and fetal pharmacokinetics in 1984 by Berglund et al. (*18*). Hartvig et al. extended these studies 5 y later and reported on fetal pharmacokinetics of ^{11}C-morphine– and ^{11}C-heroin–derived radioactivity in the placenta and fetal liver (*19*). They showed that ^{11}C-morphine was redistributed to the placenta within a few minutes and also reached the fetal liver at a high rate and calculated an apparent fetal half-life of ^{11}C-morphine of about 20 min (*19*).

The volume resolution of the PET images in the study by Hartvig et al. (*19*) was 1 cm^3, and identification of fetal anatomic structures was obviously limited because there was no corresponding anatomic MRI template for comparison. From preliminary work conducted with primates at our laboratory, we realized that it was imperative to include an MRI scan for anatomic coregistration with PET images to identify fetal organs of interest. In this first series of feasibility studies, we chose to (a) use a radioactive tracer that would provide relatively predictable tracer distribution in the mother and fetus, (b) focus on a nonquantitative whole-body PET imaging approach, (c) define suitable MR parameters for optimal display of fetal anatomy, and (d) test the use of external fiducial markers to coregister the images. Additionally, because we plan to conduct future time-course studies at various phases of gestation, it was also crucial to develop a relatively noninvasive experimental approach with anesthesia procedures that would allow full recovery of the mother and fetus.

MRI has been widely used to assess human fetal anatomy, fetal growth patterns, and fetal pathology in uteri (*21–23*). We explored several MR contrast parameters, spatial resolutions, and imaging planes to define optimal scan parameters and to assess the impact of scan-synchronous ventilation on image SNR. Because the pregnant monkeys were anesthetized with propofol, which is known to cross the placenta (*24*), fetal motion was probably minimized during image acquisitions. Of note, when acquiring MR images in unanesthetized pregnant humans, the problem of fetal motion is usually solved by decreasing the acquisition time using specialized pulse sequences (gradient-echo sequences, fast spin-echo sequences, and half-Fourier single-shot turbo spin echo, so-called HASTE sequence (*25,26*)). On the T2-weighted images acquired in our study, third-trimester fetal anatomy could be identified at spatial resolutions of 2.1–3.2 mm^3. The cerebral hemispheres, posterior lobe, and cerebellum could be identified in the fetal brains, but neither cerebral ventricles nor gray or white matter differentiation could be appreciated. In comparison, in third-trimester human fetuses, T2-weighted MR images at a volume resolution of 2.4 mm^3 readily display cerebral hemispheres, sulci, cerebellum, as well as cerebral ventricles (atria and cisterna magna) (*27*). This discrepancy is likely due to differences in the size of the macaque fetus in comparison with the human fetus and lack of spatial resolution in our images. The fetal *M. radiata* brains did not display any gray or white matter differentiation, which would indicate no myelination. In human fetal brains, the first evidence of myelination appears around 32 wk, but only in certain areas, and documentation of myelination by MRI is generally only seen postpartum (*27*). For our future fetal MRI studies, we plan to build a smaller radiofrequency coil and also incorporate more time-efficient pulse sequences, which with the same scan times used in the study will allow us to acquire images with improved spatial resolution and overall SNR. This approach will also allow us to perform studies in pregnant macaques in earlier gestational stages (for example, in this series we were not able to interpret fetal structures in the early second-trimester pregnant monkey).

Similar to the ^{18}F-FDG whole-body distribution pattern observed in humans, ^{18}F activity concentrated in the maternal macaque's brain, heart, kidneys, and bladder. SUVs for ^{18}F-FDG in brain (*28*) and peripheral organs in healthy awake humans have recently been measured using whole-body PET (*29*). For example, the cardiac (myocardium + blood pool) SUV has been reported to be 3.3. In another study (*28*), the brain SUV averaged 7.6. In our studies in the third-trimester anesthetized macaques, the maternal SUVs averaged 2.05 and 1.15 for the brain and heart, respectively, whereas the fetal brain and heart SUVs averaged 1.50 and 1.22, respectively. Thus, for the anesthetized macaques, the maternal brain-to-myocardial SUV ratio is 1.78 and the fetal brain-to-myocardial SUV ratio is 1.23. The higher brain-to-myocardial SUV in the mother most likely reflects an overall higher cerebral metabolism compared with that of the fetus. Though it is tempting to compare the SUVs and SUV ratios we have measured in the pregnant macaques with those in humans, species, pregnancy, and anesthesia variables probably account for differences and preclude quantitative comparisons.

We demonstrated that ^{18}F-FDG crosses the placenta of the nonhuman primate and accumulates in the fetus. ^{18}F-FDG is known to be transported across the placental syncytiotrophoblast basal membrane by both carrier-mediated and diffusional processes (*30*). In humans, ^{18}F-FDG is also known to cross the placenta and accumulate in the fetus (*31*). However, a systematic PET study of exactly where ^{18}F-FDG accumulates has not been performed for obvious safety and ethical reasons.

Although the gravid uterine cavity could be seen on the whole-body PET images, it was not straightforward to anatomically identify specific fetal areas of high ^{18}F activity. We therefore coregistered the PET images with the corresponding MR images and were able to demonstrate that, similarly to the mother, the fetus accumulated ^{18}F mainly in the brain, heart, and bladder. For coregistration of the 2-modality images, we used commercial software (Amira 2.3), which uses pairs of corresponding points (landmarks) on the two 3D image datasets (MRI and PET). We were able to clearly identify 18 corresponding datasets on corresponding sets of PET and MR 3D images. The 3D PET dataset was used as the master template and the MR image dataset was subsequently warped to the master template using a "nearest-neighbor interpolation approach" (rigid warp).

A wide variety of software can be used for coregistration of multimodality images (*32–35*). Surface-based fitting/warping algorithms or volume-based registration software are among the most frequently applied computational approaches. We did not systematically investigate other more sophisticated coregistration software solutions in our study but, instead, decided to focus on a computational approach that was simple (using software with a user friendly interface), not automated, and would allow us to use both external and internal landmarks for the coregistration. For future studies, it will be necessary to evaluate and test different coregistration algorithms more carefully to determine the overall spatial/anatomic accuracy of uptake measurements in the fetus and to assess the feasibility of performing studies in early gestational stages where anatomic landmarks are difficult to identify. The impact on fetal motion or fetal positional change during the study and during transports on coregistration also needs to be addressed.

The coregistration of PET and corresponding MR images revealed that the fetal brain ^{18}F activity was heterogeneous. Assuming that ^{18}F activity in the fetal brain represents ^{18}F-FDG cerebral uptake, and thus cerebral activity, the coregistration of PET and MR images demonstrated that cerebral activity was highest in the cerebellum and the forebrain of the fetus. Chugani and Phelps previously examined maturational changes in cerebral function in infants using ^{18}F-FDG PET and found that, in infants $\leq$5 wk old, glucose utilization is highest in the sensorimotor cortex, thalamus, midbrain–brain stem, and cerebellar vermis, which are in agreement with behavioral, neurophysiologic, and anatomic processes during this time in development (*36*). In this context, it is interesting that the nonhuman primate third-trimester fetuses also demonstrated high cerebellar high ^{18}F activity.

Another intriguing finding of our study was the similar maternal brain-to-fetal brain ^{18}F activity ratio of the 2 third-trimester fetuses. One interpretation of this finding could be that the anesthesia brings (propofol crosses the placenta) the maternal and fetal cerebral metabolism to a baseline required to maintain only minimal functions and the ratio is therefore constant. This would imply that greater variability in maternal brain-to-fetal brain ^{18}F activity ratios might be apparent only in the awake state. Future studies using anesthetics that penetrate the placenta less efficiently will provide answers to this question.

We implemented a carefully regulated anesthetic technique in the pregnant macaques to ensure stable physiology during the long-term imaging study as well as a rapid and uncomplicated recovery. Intravenous propofol enabled a sufficiently deep anesthetic state and, in combination with intravenous hydration and monitoring, none of the pregnant macaques developed preterm labor during or immediately after the study. Additionally, all 3 pregnant monkeys delivered normal, full-term (as evaluated by the veterinarian) babies several weeks after the experiment. There is a wide variety of anesthetic techniques that could be similarly suitable for these types of studies. However, we selected an intravenous anesthesia technique because we had to transport the macaques several times during the imaging study. Propofol allows for rapid adjustments of the anesthetic state and permits a quick recovery. It has previously been used in rhesus macaques during stereotactic frame placement and MRI (*37*). Similar to our study, the intravenous concentration of propofol used in the rhesus macaque was rather high (200–300 μg/kg/min) compared with that typically used in humans (80–150 μg/kg/min).

The prerequisite for performing future studies will obviously require access to pregnant macaques as well as also having access to a flexible and well-functioning imaging infrastructure. We are fortunate to have access to both. The primate *M. radiata* colony at SUNY Downstate, in which animals are group-housed, is able to provide us with approximately 12–16 pregnant macaques yearly at various gestational stages. Given the limited supply and the complexity of the studies, we plan to focus our future efforts on 3 areas of research: maternal–fetal transfer of cocaine and nicotine in second and third trimester, fetal drug distribution of cocaine and nicotine in second and third trimester, and fetal cocaine and nicotine transporter or receptor binding in the second and third trimester. There are clearly several technical issues that will need to be clarified when using radiotracers other than ^{18}F-FDG. For example, when using radiotracers with poor SNRs, it may be problematic to analyze fetal regions of interest in early gestational stages where the volumes or areas are intrinsically small.

Accordingly, we are currently focusing on developing dynamic scanning protocols that will enable a consistent

quantitative measure of drug pharmacokinetics using radiolabeled radiotracers such as ^{11}C-cocaine, absolute drug concentration in the brain, and transporter and receptor availability in the mother and fetus simultaneously using PET and MRI.

CONCLUSION

The pregnant macaque in combination with PET and MRI technology allows the measurement of radioisotope distribution in maternal and fetal organs. This demonstrates the potential for noninvasively measuring the transfer of drugs across the placenta and for measuring the fetal drug distribution. It also opens up the possibility for studying binding and elimination as well as the effects of a drug on specific cellular elements and physiologic processes during the gestational period in a primate model.

ACKNOWLEDGMENTS

We thank David Schlyer and Michael Schueller for cyclotron operations; Richard Ferrieri, Colleen Shea, Victor Garza, and Youwen Xu for ^{18}F-FDG preparation; and Maryann Kershaw and Kerry Bonti for primate care. This work was supported by the U.S. Department of Energy, Office of Biologic and Environmental Research, and the National Institute on Drug Abuse.

REFERENCES

1. Dyer NC, Brill AB, Raye J, Gutberle R, Stahlman M. Maternal-fetal exchange of Fe-59: radiation-dosimetry and biokinetics in human and sheep studies. *Radiat Res.* 1973;53:488–495.
2. Rosso P. Nutrition and maternal-fetal exchange. *Am J Clin Nutr.* 1981;34:744–755.
3. Lepage P, Vandeperre P, Msellati P, et al. Mother-to-child transmission of human-immunodeficiency-virus type-1 (HIV-1) and its determinants: a cohort study in Kigali, Rwanda. *Am J Epidemiol.* 1993;137:589–599.
4. Tuntland T, Odinecs A, Pereira CM, Nosbisch C, Unadkat JD. In vitro models to predict the in vivo mechanism, rate, and extent of placental transfer of dideoxynucleoside drugs against human immunodeficiency virus. *Am J Obstet Gynecol.* 1999;180:198–206.
5. Chamberlain G. Placental transfer of drugs. *Clin Exp Obstet Gynecol.* 1986;13:107–112.
6. Sastry BVR. Techniques to study human placental transport. *Adv Drug Deliv Rev.* 1999;38:17–39.
7. Jansson T, Powell TL. Placental nutrient transfer and fetal growth. *Nutrition.* 2000;16:500–502.
8. Dalterio SL. Cannabinoid exposure: effects on development. *Neurobehav Toxicol Teratol.* 1986;8:345–352.
9. Krug SE. Cocaine abuse: historical, epidemiologic, and clinical perspectives for pediatricians. *Adv Pediatr.* 1989;36:369–406.
10. Levy M, Koren G. Obstetric and neonatal effects of drugs of abuse. *Emerg Med Clin North Am.* 1990;8:633–652.
11. Schenker S, Yang YQ, Johnson RF, et al. The transfer of cocaine and its metabolites across the term human placenta. *Clin Pharmacol Ther.* 1993;53:329–339.
12. Ganapathy V, Prasad PD, Ganapathy ME, Leibach FH. Placental transporters relevant to drug distribution across the maternal-fetal interface. *J Pharmacol Exp Ther.* 2000;294:413–420.
13. Kan RE, Hughes SC, Rosen MA, Kessin C, Preston PG, Lobo EP. Intravenous remifentanil: placental transfer, maternal and neonatal effects. *Anesthesiology.* 1998;88:1467–1474.
14. Hostetter A, Ritchie JC, Stowe ZN. Amniotic fluid and umbilical cord blood concentrations of antidepressants in three women. *Biol Psychiatry.* 2000;48:1032–1034.
15. Brace RA. Physiology of amniotic fluid volume regulation. *Clin Obstet Gynecol.* 1997;40:280–289.
16. Patterson TA, Binienda ZK, Lipe GW, Gillam MP, Slikker W Jr, Sandberg JA. Transplacental pharmacokinetics and fetal distribution of azidothymidine, its glucuronide, and phosphorylated metabolites in late-term rhesus macaques after maternal infusion. *Drug Metab Dispos.* 1997;25:453–459.
17. Nicklas AH, Baker ME. Imaging strategies in the pregnant cancer patient. *Semin Oncol.* 2000;27:623–632.
18. Berglund L, Halldin C, Lilja A, et al. ^{11}C-Methionine kinetics in pregnant rhesus monkeys studied by positron emission tomography: a new approach to fetomaternal metabolism. *Acta Obstret Gynecol Scand.* 1984;63:641–645.
19. Hartvig P, Lindberg BS, Lilja A, Lundqvist H, Langstrom B, Rane A. Positron emission tomography in studies on fetomaternal disposition of opioids. *Dev Pharmacol Ther.* 1989;12:74–80.
20. Hammacher K, Coenen HH, Stocklin G. Stereospecific synthesis of NCA 2-[^{18}F]fluoro-2-deoxy-2-D-glucose using aminopolyether supported nucleophilic substitution. *J Nucl Med.* 1986;27:235–238.
21. Garden AS, Roberts N. Fetal and fetal organ volume estimations with magnetic resonance imaging. *Am J Obstet Gynecol.* 1996;175:442–448.
22. Garel C, Chantrel E, Brisse H, et al. Fetal cerebral cortex: normal gestational landmarks identified using prenatal MR imaging. *AJNR.* 2001;22:184–189.
23. Levine D, Trop I, Mehta TS, Barnes PD. MR imaging appearance of fetal cerebral ventricular morphology. *Radiology.* 2002;223:652–660.
24. Sanchez-Alcaraz A, Quintana MB, Laguarda M. Placental transfer and neonatal effects of propofol in caesarean section. *J Clin Pharm Ther.* 1998;23:19–23.
25. Levine D, Hatabu H, Gaa J, Atkinson MW, Edelman RR. Fetal anatomy revealed with fast MR sequences. *AJR.* 1996;167:905–908.
26. Yamashita Y, Namimoto T, Abe Y, et al. MR imaging of the fetus by a HASTE sequence. *AJR.* 1997;168:513–519.
27. Trop I, Levine D. Normal fetal anatomy as visualized with fast magnetic resonance imaging. *Top Magn Reson Imaging.* 2001;12:3–17.
28. Shigeru Y, Ishii K, Sasaki M, et al. Evaluation of standardized uptake value to assess cerebral glucose metabolism. *Clin Nucl Med.* 2000;25:11–16.
29. Ramos CD, Erdi YE, Gonen M, et al. FDG-PET standardized uptake values in normal anatomical structures using iterative reconstruction segmented attenuation correction and filtered back-projection. *Eur J Nucl Med.* 2001;28:155–164.
30. Quraishi AN, Illsley NP. Transport of sugars across human placental membranes measured by light scattering. *Placenta.* 1999;20:167–174.
31. Adelstein SJ. Administered radionuclides in pregnancy. *Teratology.* 1999;59:236–239.
32. Lamm C, Windischberger C, Leodolter U, Moser E, Bauer H. Co-registration of EEG and MRI data using matching of spline interpolated and MRI-segmented reconstructions of the scalp surface. *Brain Topogr.* 2001;14:93–100.
33. Barnden L, Kwiatek R, Lau Y, et al. Validation of fully automatic brain SPET to MR co-registration. *Eur J Nucl Med.* 2000;27:147–154.
34. Sakiyama Y, Toyama H, Oda K, et al. A stereotaxic method of anatomical localization by means of $H_2{}^{15}O$ positron emission tomography applicable to the brain activation study in cats: registration of images of cerebral blood flow to brain atlas. *Ann Nucl Med.* 1997;11:315–319.
35. Singh KD, Holliday IE, Furlong PL, Harding GF. Evaluation of MRI-MEG/EEG co-registration strategies using Monte Carlo simulation. *Electroencephalogr Clin Neurophysiol.* 1997;102:81–85.
36. Chugani HT, Phelps ME. Maturational changes in cerebral function in infants determined by ^{18}FDG positron emission tomography. *Science.* 1986;231:840–843.
37. Fowler KA, Huerkamp MJ, Pullium JK, Subramanian T. Anesthetic protocol: propofol use in rhesus macaques (*Macaca mulatta*) during magnetic resonance imaging with stereotactic head frame application. *Brain Res Brain Res Protoc.* 2001;7:87–93.